Manfred Tillich, MD[2]
Rebecca E. Bell, MD[3]
David S. Paik, MS
Dominik Fleischmann, MD[4]
Marc C. Sofilos, RT
Laura J. Logan, RT
Geoffrey D. Rubin, MD

Index terms:
Aneurysm, abdominal, 981.73
Arteries, iliac, 984.458
Computed tomography (CT), angiography, 98.12912, 98.12915, 98.12916
Interventional procedures, complications
Stents and prostheses

Radiology 2001; 219:129–136

Abbreviation:
CSA = cross-sectional area

[1] From the Department of Radiology, Stanford University School of Medicine, S-072B, 300 Pasteur Dr, Stanford, CA 94305-5105. Received March 9, 2000; revision requested April 26; revision received August 8; accepted August 11. **Address correspondence to** G.D.R. (e-mail: *grubin@stanford.edu*).

Current addresses:
[2] Department of Radiology, University of Graz, Austria.
[3] Department of Pediatrics, Georgetown University School of Medicine, Washington, DC.
[4] Department of Radiology, University Hospital, Vienna, Austria.

Author contributions:
Guarantors of integrity of entire study, M.T., G.D.R.; study concepts and design, G.D.R.; definition of intellectual content, M.T., D.S.P., G.D.R.; literature research, M.T.; clinical studies, M.C.S., L.J.L.; data acquisition, M.T., R.E.B., M.C.S., L.J.L., D.F.; data analysis/interpretation, M.T., G.D.R.; statistical analysis, M.T.; manuscript preparation, M.T., D.S.P.; manuscript editing, G.D.R.; manuscript revision/review, M.T.; manuscript final version approval, G.D.R.

Iliac Arterial Injuries after Endovascular Repair of Abdominal Aortic Aneurysms: Correlation with Iliac Curvature and Diameter[1]

PURPOSE: To determine the relationship between iliac arterial tortuosity and cross-sectional area and the occurrence of iliac arterial injuries following transfemoral delivery of endovascular prostheses for repair of abdominal aortic aneurysms.

MATERIALS AND METHODS: Iliac arterial curvature values and orthogonal cross-sectional areas were determined from helical computed tomographic (CT) data acquired in 42 patients prior to transfemoral delivery of aortic stent-grafts. The curvature and luminal cross-sectional area orthogonal to the median centerline were quantified every millimeter along the median centerline of the iliac arteries. An indicator of global iliac tortuosity, the iliac tortuosity index, was defined as the sum of the curvature values for all points with a curvature of 0.3 cm^{-1} or greater, and cross-sectional area (CSA) was indexed for all points as the mean cross-sectional diameter ($\bar{D} = 2\sqrt{[CSA/\pi]}$). Following stent-graft deployment, helical CT data were analyzed for the presence of iliac arterial dissections independently by two reviewers.

RESULTS: Eighteen dissections were detected in 16 patients. The iliac tortuosity index was significantly larger in iliac arteries with dissections (35.5 ± 20.8 [mean ± SD]) when compared with both nondissected contralateral iliac arteries in the same patients (26.1 ± 21.0, $P = .001$) and iliac arteries in patients without any iliac arterial injury (20 ± 9, $P = .009$). The tortuosity index was higher ipsilateral to the primary component delivery in 10 of 11 iliac dissections that developed along the primary component delivery route.

CONCLUSION: A high degree of iliac arterial tortuosity appears to impart greater risk for the development of iliac arterial injuries in patients undergoing transfemoral delivery of endovascular devices.

Abdominal aortic aneurysms are often associated with narrow and tortuous iliac arteries (1–8). This relationship may have important implications concerning the technique of endovascular repair of abdominal aortic aneurysms.

The major shortcoming of transverse computed tomographic (CT) images is in the evaluation of the iliac arteries because elongation and tortuosity of the artery may result in a parallel or tangential course of the vessel relative to the image plane that may preclude accurate assessment of lumen diameter and plaque morphology (9). Conventional arteriography is limited, however, by its inability to demonstrate the vessel wall and by the effects of projection, magnification, and parallax on the accuracy of quantitative evaluation (10,11).

The planning of endovascular repair of abdominal aortic aneurysms puts greater requirements on preoperative imaging because it must provide accurate information about the morphologic characteristics and quantitative dimensions of the arterial segments involved. Another important issue in the preoperative evaluation of patients is to determine the appropriate access route for device delivery. The spectrum of possible complications ranges from failure to deliver the stent-graft to atheroembolism and intimal injury (12–17). An accurate quantitative evaluation of the diameter and curvature of the iliac

arteries, as well as morphologic characterization of the vessel wall prior to stent-graft deployment may prove critical to identifying the optimal delivery route.

This study was conducted to test the following two hypotheses: Our first hypothesis was that larger iliac arterial curvature increases the risk for intimal injury or rupture during stent-graft deployment. Our second hypothesis was that intimal injuries to the iliac arteries are associated with smaller iliac arterial diameters.

MATERIALS AND METHODS

Patient Population

Forty-two consecutive patients (38 men and four women; age range, 45–89 years; mean age, 69 years) with infrarenal abdominal aortic aneurysms underwent helical CT before and after endovascular stent-graft deployment. These examinations were part of our routine clinical protocol for predeployment evaluation and postdeployment follow-up. Two types of endovascular nitinol-polyester stent-grafts were used: An AneuRx stent-graft (Medtronic, Santa Rosa, Calif) was deployed in 40 patients, and a Prograft stent-graft (Gore, Flagstaff, Ariz), in two patients. A bifurcated graft was used in 41 patients, and a tube graft, in one patient.

All devices were composed of a self-expanding nitinol skeleton covered with woven polyester graft material. Both bifurcated devices were composed of a primary device that contains the aortic and ipsilateral iliac limbs and a secondary device that is introduced through the contralateral femoral artery and that contains the other iliac limb. The diameters of the AneuRx primary and secondary device components with introducers were 22 and 16 F, respectively. The diameters of the Prograft primary and secondary device components with introducers were 18 and 12 F, respectively. The primary site of stent-graft deployment was chosen on the basis of visual analysis of three-dimensional CT angiograms and/or conventional angiograms. Quantitative volumetric analysis was not available prior to stent-graft deployment.

The mean intervals between pre- and postdeployment helical CT relative to stent-graft deployment were 23 days ± 12 (SD) and 2 days ± 1, respectively.

Imaging Techniques

CT data were obtained with one of two helical CT scanners (CTi, GE Medical Systems, Milwaukee, Wis; Somatom Plus 4, Siemens Medical Systems, Iselin, NJ). CT angiography was performed to image from the celiac origin to the bifurcation of the femoral arteries in a single acquisition. To define the imaging volume of interest, nonenhanced localizing scans were obtained with 10-mm collimation and a pitch of 2.0. Subsequently, a 20-gauge antecubital intravenous catheter was positioned and flushed with saline to ensure that it could safely allow an infusion rate of 4 mL/sec.

The scanning delay was determined following intravenous injection of 15 mL of low-osmolar contrast medium (iohexol [Omnipaque 300]; Nycomed, Princeton, NJ) injected at a rate of 4 mL/sec. Eight seconds after initiation of the test injection, single-level CT images were obtained every 2 seconds at the level of the supraceliac aorta. A total of 15 sections were obtained, and regions of interest were placed within the abdominal aorta by CT technologists, resulting in a time-attenuation curve. The interval between the start of the injection and maximum contrast enhancement of the aorta was selected as the delay time for acquisition of the ensuing CT angiogram.

Patients were instructed to hold their breath for a total of 30 seconds while the aorta and proximal iliac arteries were imaged. They were then allowed to breathe quietly during the terminal portion of the 40–50-second acquisition while the midiliac and distal iliac arteries were imaged within the pelvis, where respiratory misregistration was not substantial.

CT angiography was performed with a gantry rotation of 1.0 second for CTi (GE Medical Systems) scans and 0.75 second for Somatom Plus 4 (Siemens) scans. Three-millimeter collimation and a pitch of 2.0 was used to the distal abdominal aorta. For all 1.0-second gantry rotation scans, this step was followed by a required 5-second interruption to change collimation, and scanning was resumed with 5-mm collimation and a pitch of 2.0 until the lesser femoral trochanter was reached. Breath holding was maintained during the 5-second interruption to avoid misregistration. Three-millimeter collimation was used throughout the entire acquisition of 0.75-second gantry rotation scans. Low–osmolar contrast medium was injected at a flow rate of 4 mL/sec, and a volume of 140–180 mL of contrast medium was delivered to establish a bolus duration that was equivalent to the scanning duration. The data were reconstructed every 2.0 mm with a 180° linear interpolation algorithm and a longitudinal field of view equivalent to the total travel distance (38–44 cm) of the table.

Image Analysis

All postdeployment helical CT studies were evaluated independently for iliac arterial dissections on a commercially available CT workstation (Autorad; CemaxIcon, Mountain View, Calif) by two radiologists (M.T., G.D.R.). An intimal injury was diagnosed when an intimal flap was visible below the most distal aspect of the stent-graft within the flow lumen of the iliac arteries, which was not visible on predeployment CT images. Furthermore, the relationship between the intimal flap and the presence of iliac arterial wall calcifications was evaluated. When discrepancies existed between the two reviewers, they were resolved by consensus.

The length of the dissected arterial segment was measured along the median centerline of the iliac flow lumen, and the distance between the dissection and neighboring arterial branches was recorded. Iliac dissections that extended into the common femoral artery were classified as iliofemoral dissections, whereas those involving an iliac segment alone were classified as iliac segment dissections.

Volumetric Analysis with CT Angiograms

All pre- and postdeployment image data were transferred to a computer workstation (O2; Silicon Graphics, Mountain View, Calif) with an R12000 processor chip (300-MHz processor) and 1,024 Mbytes of RAM. Linear interpolation was performed to create isotropic voxels. The contrast material–enhanced flow channel was extracted by means of three-dimensional region growing (18,19). A point within the supraceliac aorta and within the common femoral arteries was manually selected to define the limits of calculation of the median luminal centerline for the aorta and each iliac artery. The median centerline was computed by means of a median axis transform, which is a morphologic operation that thins the segmented flow channel from the outside in; what remains is a connected set of points that define the median axes through the aorta and the iliac arteries (20).

Orthogonal cross sections were created every millimeter along the path. The path was smoothed by means of a Hanning filter to provide closed-form expressions of local derivatives along the path, which allowed us to calculate the curvature (K) at discrete intervals along the median centerline as a function of the longitudinal position along the vessel of interest. The curvature (K) was specifically defined as the inverse of the radius

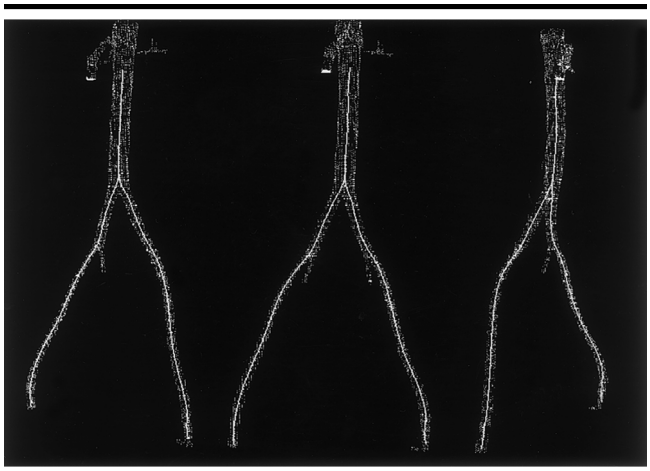

a.

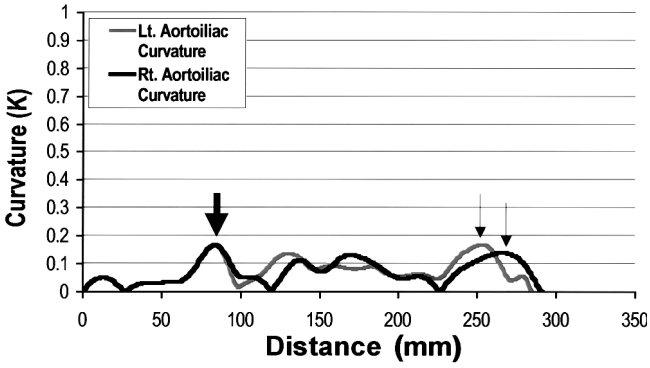

b.

Figure 1. Helical CT angiogram obtained in a 25-year-old patient after a motor vehicle accident shows a normal aorta and iliac arteries. **(a)** Left anterior oblique (left), anteroposterior (middle), and right anterior oblique (right) views of the aorta and iliac arteries with median centerlines. **(b)** Corresponding plots of curvature versus distance from the renal artery origins through the common femoral arteries. The maximum curvature (0.17 cm^{-1}) occurs at the aortic bifurcation (thick arrow), with distal secondary peaks as the femoral arteries course over the femoral heads (thin arrows). Because there are no curvature values of 0.3 cm^{-1} or greater, the tortuosity indices are zero for the two iliac arteries.

of the curvature (in centimeters^{-1}) and was calculated as $K = \|\mathbf{X}' \times \mathbf{X}''\|/\|\mathbf{X}'\|^3$, where $\|\mathbf{X}'\|$ is the magnitude of the first derivative vector of the path, $\mathbf{X}''$ is the second derivative vector of the path, and the multiplication cross denotes the vector cross product. A more complete description of these methods and their validation can be found in an article by Rubin et al (20).

To develop an overall iliac arterial tortuosity index, a consensus panel composed of two vascular surgeons and the two radiologists reviewed three-dimensional renderings of CT scans from eight patients with abdominal aortic aneurysms who were not included in the study group. The images were reviewed to assess a lower limit for iliac arterial curvature that was perceived as representing a region of local tortuosity. This analysis was performed by consensus with the four physicians interactively correlating the plot of aortoiliac curvature with the corresponding location on the three-dimensional renderings. Curvature values less than 0.3 cm^{-1}, corresponding to radii of curvature of greater than 3.3 cm, were not associated with sites of visually perceptible local arterial tortuosity. Therefore, all values of curvature less than 0.3 cm^{-1} were ignored, and an overall index of tortuosity was calculated as the sum of all curvature values measured every millimeter along the length of the iliac arteries that were 0.3 cm^{-1} and higher. The purpose of ignoring small, imperceptible curvature values was to avoid biasing high tortuosity index values toward longer, but not necessarily more tortuous, arteries. A healthy patient should have a tortuosity index of 0 (Fig 1).

The orthogonal cross-sectional areas (CSAs) along the aorta and the iliac arteries were calculated by using a threshold–based two-dimensional region-growing algorithm. Rather than use a fixed threshold as in reference 20, we used an adaptive method that sets a threshold at each position along the centerline based on the intensity histogram within a sphere of interest that travels along the path (21). By using both curved and straight acrylic tubes filled with solutions of varying attenuation, we previously determined that a lower threshold equal to 92.5% of the mean attenuation within a 4-mm diameter sphere of interest results in an error of less than 0.25 mm^2 for CSA measurements in simulated blood vessels with absolute luminal diameters 2.7–15.8 mm. We expressed luminal CSA as the mean cross-sectional diameter at each point as $\bar{D} = 2\sqrt{(CSA/\pi)}$.

The entire CT analysis required 15–20 minutes.

Statistical Analysis

Iliac arteries were stratified into one of three groups: those with intimal dissections, undissected arteries contralateral to dissected iliac arteries, and arteries in patients who did not have iliac arterial dissection. Volumetric analysis of the undissected contralateral iliac arteries was performed to evaluate the relationship between minimum diameter, maximum curvature, and iliac tortuosity index of the dissected iliac artery. Subsequently, these data were correlated with the location of primary and secondary site of stent-graft deployment. The mean and SD of the maximum curvature and the tortuosity index were calculated for each group. Unpaired two-sample *t* tests were used to determine if the maximum curvature, tortuosity index, and minimum iliac diameter measurements of dissected iliac arteries were significantly different among the groups. A *P* value less than .05 was considered to indicate a statistically significant difference.

RESULTS

A total of 18 acute iliac arterial dissections was found in 16 patients, resulting in a prevalence of 0.21 for the 84 analyzed iliac arteries. The dissections were located on the primary site of stent-graft deployment in 11 (69%) patients, on the secondary site in three (19%) patients, and bilaterally in two (12%) patients. Bi-

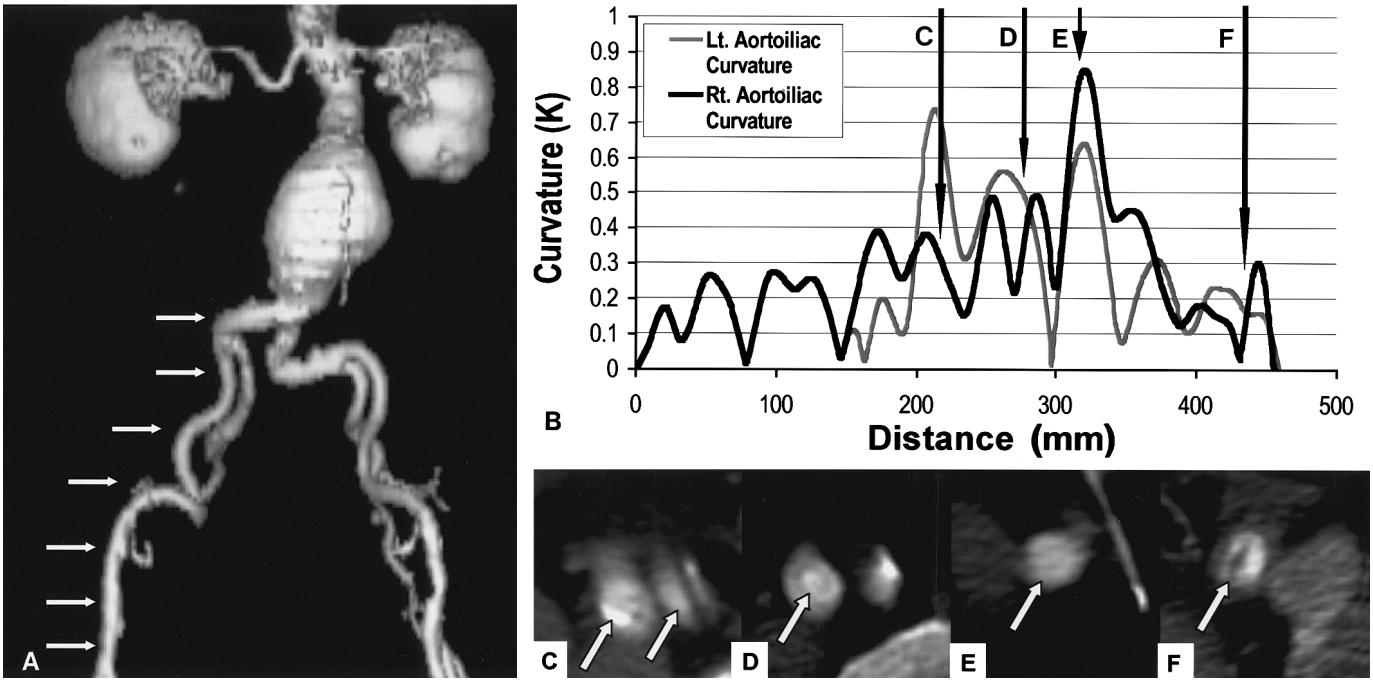

Figure 2. Helical CT angiographic data obtained in an 82-year-old man with an abdominal aortic aneurysm before (*A*, *B*) and after (*C–F*) deployment of a bifurcated stent-graft. *A*, Anteroposterior shaded-surface display of the predeployment data shows the abdominal aortic aneurysm and tortuous iliac arteries. Maximum curvature and the tortuosity index were higher on the right side, which was the primary site of stent-graft deployment. The maximum curvature measured 0.85 versus 0.75 cm^{-1}, while the tortuosity index measured 68 versus 66 for the dissected right versus the nondissected left iliac arteries, respectively. Arrows indicate the extent of the postprocedural long segment dissection from the right common iliac artery bifurcation to the common femoral artery. *B,* Aortoiliac curvature is plotted as a function of distance along the median centerline of the flow lumen of the aorta and iliac arteries. The aortic bifurcation corresponds to the point where the two curves diverge. Arrows at *C–F* correspond to sections in *C–F*. *C–F,* Transverse CT sections through the right iliac artery correspond to positions indicated by arrows at *C–F* in *B*. Arrows indicate the intimal flap within the lumen of the external and internal iliac and common femoral arteries. Note also the intimal flap within the internal iliac artery in *C*.

lateral dissections were found in two patients after deployment of a bifurcated stent-graft. The length of the dissected iliac segment ranged from 10 to 215 mm, with a mean of 85 mm ± 66.

Iliofemoral Dissections

In four dissections, the intimal flap extended from the common femoral artery to the distal fixation site of the stent-graft limb, and in two, it extended from the common femoral artery to the common iliac bifurcation (Fig 2). The dissected arterial segment encompassed the point of maximum iliac arterial curvature in all patients. The maximum curvature ranged from 0.35 to 0.85 cm^{-1}, with a mean of 0.54 cm^{-1} ± 0.15, and the tortuosity index ranged from 11.1 to 68.0, with a mean of 35.4 ± 23.3. The minimum mean diameter of the dissected arterial segment ranged from 5 to 7 mm, with a mean of 6.0 mm ± 0.7.

Iliac Dissections

The intimal flap was located in the distal segment of the external iliac artery in two patients, in the proximal segment of the external iliac artery in nine patients, and at the common iliac artery in one patient (Figs 3, 4). Lengths ranged from 10 to 86 mm, with a mean of 48 mm ± 28. All dissection flaps originated from the greater curve of the vessel wall. A calcified atherosclerotic plaque was detected at the distal aspect of the intimal flap in five of 12 patients.

The maximum curvature of the dissected segment of the iliac arteries ranged from 0.35 to 0.85 cm^{-1}, with a mean of 0.51 cm^{-1} ± 0.13 and occurred at the point of maximum iliac curvature in eight of 12 dissections. In three cases, the maximum iliac curvature was located 25–33 mm (mean, 29 mm ± 3) proximal to the dissected vessel segment, and in one case, it was located 25 mm distal to the dissected vessel segment. Among these vessels, the tortuosity index ranged from 15.0 to 62.8, with a mean of 35.6 ± 19.4. The minimum diameter of the dissected arterial segment ranged from 5 to 12 mm, with a mean of 8.5 mm ± 1.6.

Nondissected Vessels

The maximum curvature of nondissected iliac arteries contralateral to dissected iliac arteries (n = 16) was 0.26–0.75 cm^{-1}, with a mean of 0.52 cm^{-1} ± 0.16. The tortuosity index for these vessels was 0 to 66.9, with a mean of 26.1 ± 21.0, and the minimum diameter of these vessels was 6–9 mm, with a mean of 6.8 mm ± 1.1. The maximum curvature of iliac arteries in patients without any iliac arterial dissection (n = 18) was 0.25–0.70 cm^{-1}, with a mean of 0.46 cm^{-1} ± 0.12. The tortuosity index for these vessels was 0–38.9, with a mean of 19.9 ± 10.5, and the minimum diameter of these vessels was 4–8 mm, with a mean of 6.8 mm ± 0.9.

Comparison of Dissected with Nondissected Iliac Arteries

A comparison of the maximum curvature and tortuosity index between the dissected and nondissected iliac arteries revealed that the maximum curvature and the tortuosity index were larger on the dissected site in 12 and 13 of 14 patients with unilateral dissections, respectively. The mean maximum curvature of the dissected iliac arteries was larger (0.56

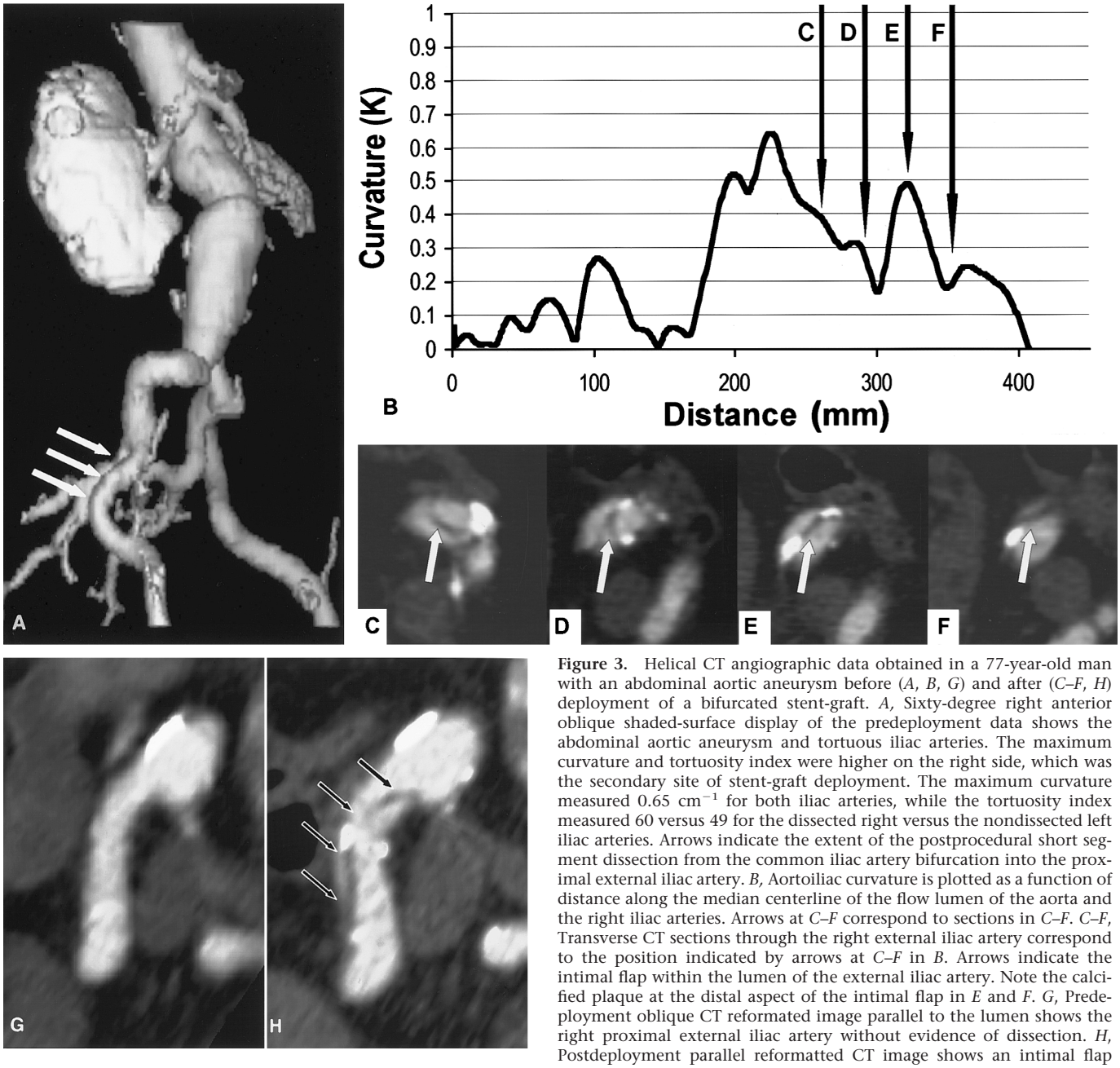

Figure 3. Helical CT angiographic data obtained in a 77-year-old man with an abdominal aortic aneurysm before (*A*, *B*, *G*) and after (*C–F*, *H*) deployment of a bifurcated stent-graft. *A,* Sixty-degree right anterior oblique shaded-surface display of the predeployment data shows the abdominal aortic aneurysm and tortuous iliac arteries. The maximum curvature and tortuosity index were higher on the right side, which was the secondary site of stent-graft deployment. The maximum curvature measured 0.65 cm^{-1} for both iliac arteries, while the tortuosity index measured 60 versus 49 for the dissected right versus the nondissected left iliac arteries. Arrows indicate the extent of the postprocedural short segment dissection from the common iliac artery bifurcation into the proximal external iliac artery. *B,* Aortoiliac curvature is plotted as a function of distance along the median centerline of the flow lumen of the aorta and the right iliac arteries. Arrows at *C–F* correspond to sections in *C–F*. *C–F*, Transverse CT sections through the right external iliac artery correspond to the position indicated by arrows at *C–F* in *B*. Arrows indicate the intimal flap within the lumen of the external iliac artery. Note the calcified plaque at the distal aspect of the intimal flap in *E* and *F*. *G*, Predeployment oblique CT reformated image parallel to the lumen shows the right proximal external iliac artery without evidence of dissection. *H*, Postdeployment parallel reformatted CT image shows an intimal flap (arrows) within the right proximal external iliac artery.

cm^{-1} ± 0.15) than for the nondissected contralateral iliac arteries (0.52 cm^{-1} ± 0.16) and for the patients without iliac dissections (0.46 cm^{-1} ± 0.12) (Table); the differences were not significant (P = .12 and .06, respectively). However, the tortuosity index was significantly larger (35.5 ± 20.8) for the dissected iliac arteries than for the contralateral nondissected iliac arteries (26.1 ± 21.0) and larger than for iliac arteries in patients without iliac dissections (19.9 ± 10.5) (P = .001 and .009, respectively).

Although the mean diameter of dissected iliac arteries (6.5 mm ± 0.6) was smaller than that of nondissected arteries (7.1 mm ± 0.9), this difference was not statistically significant (P = .08).

Tortuosity Index: Comparison of the Primary and Secondary Sites of Stent-Graft Deployment

For patients with unilateral dissections, the primary delivery route of the stent-graft was on the right in 10 and on the left in four. For patients without dissections, the primary delivery route of the stent-graft was on the right in 14 and on the left in 12. For all 42 patients, the tortuosity index of the right iliac artery averaged 1.8 higher than that of the left; the difference was not significant (P = .37).

A dissection was found on the side in which the primary stent-graft component was delivered in 11 patients. The tortuosity index of the primary delivery route was larger than on the nondissected secondary route in 10 of 11 patients. In these 10 pa-

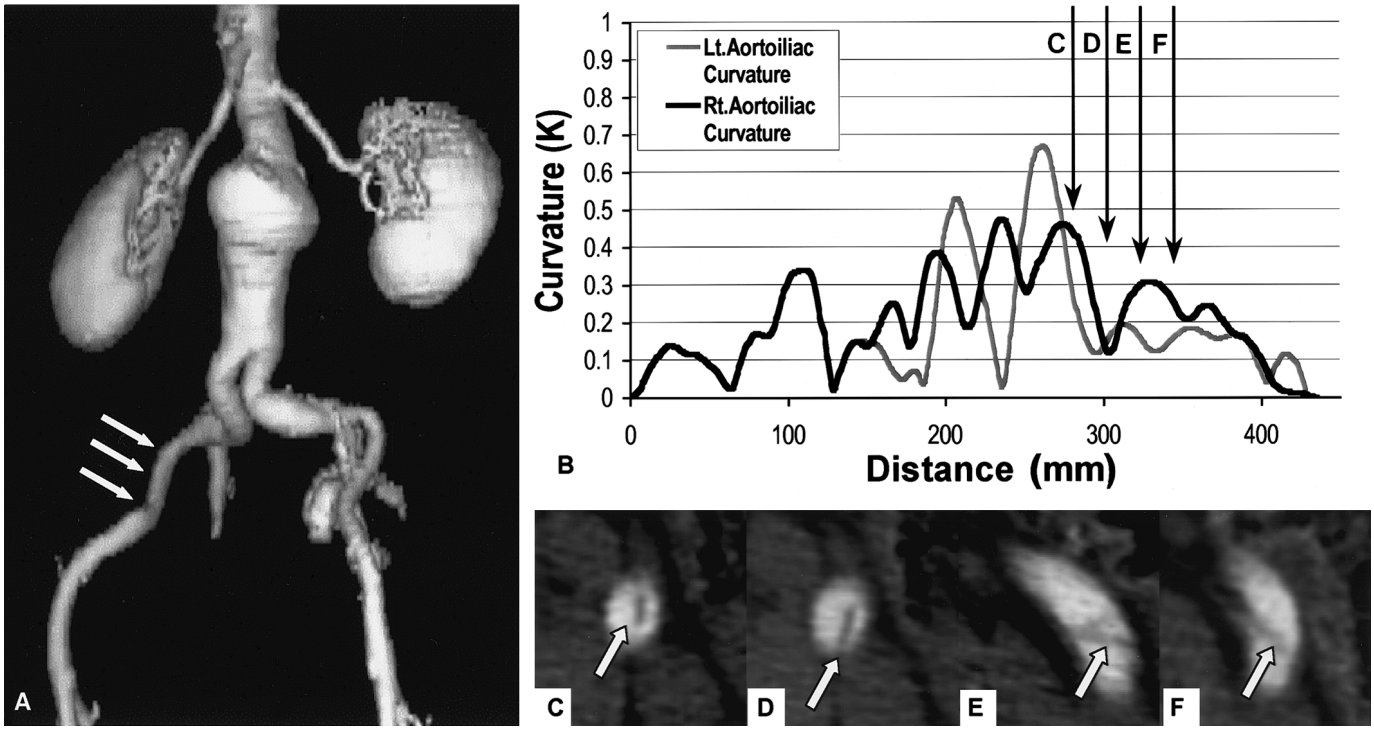

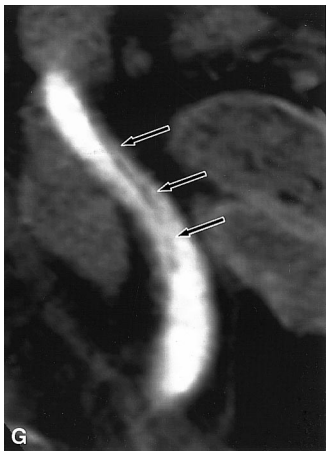

Figure 4. Helical CT angiographic data obtained in a 77-year-old man with an abdominal aortic aneurysm before (*A*, *B*) and after (*C–F*) deployment of a bifurcated stent-graft. *A*, Fifteen-degree left anterior oblique shaded-surface display of the predeployment data shows the abdominal aortic aneurysm and tortuous iliac arteries. The maximum curvature was higher on the left side, whereas the tortuosity index was higher on the right side, which was the primary site of stent-graft deployment. The maximum curvature measured 0.45 versus 0.65 cm^{-1}, while the tortuosity index measured 40 versus 31 for the dissected right versus the nondissected left iliac arteries. Arrows indicate the extent of the postprocedural short segment dissection in the right external artery. *B*, Aortoiliac curvature is plotted as a function of distance along the median centerline of the flow lumen of the aorta and the iliac arteries. Arrows at *C–F* correspond to sections in *C–F*. *C–F*, Transverse CT sections through the right external iliac artery correspond to the positions indicated by arrows at *C–F* in *B*. Arrows indicate the intimal flap within the lumen of the external iliac artery. *G*, Postdeployment parallel reformatted CT image shows an intimal flap (arrows) within the right proximal external iliac artery.

Iliac Artery Curvatures, Tortuosity Indices, and Diameters

Value	Dissected Iliac Arteries	Nondissected Arteries in Patients with Contralateral Dissection	Iliac Arteries in Patients without Dissection
Maximum curvature (cm^{-1})*	0.56 ± 0.15	0.52 ± 0.16	0.46 ± 0.12
Tortuosity index†	35.5 ± 20.8	26.1 ± 21.0	19.9 ± 10.5
Smallest mean diameter (mm)*	6.5 ± 0.6	6.8 ± 1.0	7.1 ± 0.9

Note.—All values are the mean plus or minus the SD.
* Values for maximum curvature and minimum diameter were not significantly different.
† Tortuosity index was significantly larger for the dissected iliac arteries than for the contralateral nondissected iliac arteries and larger than for iliac arteries in patients without dissection ($P = .001$ and .009, respectively).

tients, the increase in tortuosity index between the dissected primary site and the nondissected secondary site ranged from 0.6 to 17.3, with a mean of 6.5 ± 4.8 ($P = .002$). In one patient, the tortuosity index was 4.1 greater in the nondissected secondary deployment site than in the dissected primary site.

While the tortuosity index of the primary delivery route was higher in 10 of 11 patients with primary delivery route dissections, the tortuosity index of the primary delivery route was higher in only seven of 29 patients without primary delivery route dissections. In these patients, the primary versus secondary delivery route tortuosity index difference was not significantly different ($P = .21$).

For patients in whom the primary delivery route corresponded to the iliac artery with the higher tortuosity index, the mean tortuosity index was 31.5 and 23.1 for patients with and without primary delivery route dissections, respectively. Overall, the likelihood of primary delivery route dissection was 64% (nine of 14 patients), 20% (four of 20 patients), and 0% (zero of eight patients) if the primary delivery route had a tortuosity index of greater than 2.9, 1.1–2.7, or less than 0.72, respectively.

For the three patients in whom dissections

occurred in the secondary site of stent-graft deployment, the tortuosity index was larger than in the nondissected primary side. The index increase ranged from 10.1 to 16.3, with a mean of 13.5 ± 2.6.

DISCUSSION

When the aortoiliac system is assessed prior to stent-graft repair, four discrete regions can be defined that have features relevant to the delivery, fixation, and ultimate sealing of the stent-graft. They are the proximal neck, aneurysm body, distal neck, and delivery route. This study quantitatively addressed two important properties of the delivery route: iliac arterial diameter and tortuosity. To our knowledge, this is the first investigation in which iliac arterial tortuosity in a clinical cohort was quantified and correlated with clinical outcomes.

Factors that should influence the selection of the primary access route for aortic stent-grafts are diameter, tortuosity, and atherosclerotic plaque morphologic characteristics of the iliac arteries. Potential deployment problems may be failed device delivery, the need for excessive force to advance the device, atheroembolism, and intimal injury (12–17).

The results of this study demonstrated that a tortuosity index, defined as the sum of all iliofemoral curvature values every millimeter along the vessel that are greater than 0.3, was significantly larger in dissected arteries when compared with nondissected arteries. Although the maximum iliac curvature of dissected iliac arteries was larger than in nondissected iliac arteries, the difference was not significant. The observation that the maximum curvature and tortuosity index were larger on the dissected side in 14 and 15 of 16 dissections, respectively, supports the conclusion that the risk of dissection from stent-graft delivery is higher in tortuous iliac arteries.

Perhaps more relevant to the planning of stent-graft delivery is the observation that the tortuosity index of the primary delivery route was larger than that of the nondissected secondary route in 10 of 11 patients. This indicates one of two things: (*a*) that current stent-graft delivery does not rely substantially on avoiding the more tortuous of the two transileofemoral delivery routes or (*b*) that iliofemoral tortuosity cannot be determined accurately from current image-based analyses. Intimal injuries might be reduced if stent-graft delivery were accomplished through the less tortuous route.

The rationale for creating a tortuosity index that was determined as the sum of all curvature values greater than a set threshold was to integrate the curvature across the entire length of the iliac arteries, to provide a measure of cumulative curvature. Curvature values less than 0.3 were excluded to avoid skewing tortuosity index values higher in long iliac arteries that are not necessarily tortuous. Our findings support a hypothesis that increased cumulative iliac arterial curvature, measured by using the tortuosity index, is associated with an increased risk of intimal injury in endovascular repair of abdominal aortic aneurysms. A specific relationship between tortuosity index, maximum curvature, and mural shear forces that presumably increase the risk of intimal injuries awaits elucidation through further investigation.

Intimal injuries are a common complication of endovascular manipulation, although the frequency of this complication after stent-graft deployment is not clearly stated in the literature (12,15,22–24). In our study group, eight (44%) of 18 iliac dissections were associated with calcified atherosclerotic plaques (Fig 3). Waller et al (23) evaluated the relationship between the degree of vascular calcification and the extent of injury caused by percutaneous transluminal coronary angioplasty. They concluded that heavily calcified vessels were the most susceptible to extensive injury.

In the series reported by Becker et al (22), all dissected iliac arteries had radiographically visible calcification. Although we did not specifically quantify mural calcium in this study, the methods that we used to quantify curvature and diameter are applicable to an analysis of calcifications as well. The challenge of endovascular-device delivery of rigid, large-diameter introducer sheaths associated with current-generation stent-grafts through small, tortuous vessels has been previously recognized. Methods currently in use to address this challenge involve the insertion of the delivery system through the distal common iliac artery (25) or the use of a pull-down maneuver to straighten the iliac artery by applying inferior traction following dissection of the common femoral and external iliac arteries (26). Both procedures are more invasive and time-consuming than standard Seldinger techniques for advancing the device.

In conclusion, we have developed a method for quantifying iliac tortuosity that is based on a true three-dimensional assessment of the arterial lumen and that is independent of view-dependent measurements that result when two-dimensional projections are assessed. The magnitude of tortuosity measured with our tortuosity index is highly correlative with the likelihood for intimal injuries occurring in the iliac arteries following stent-graft delivery. These observations may have relevance to the selection of delivery routes for stent-graft deployment. This is particularly true in light of our findings that the larger primary device component of a bifurcated system was delivered through the more tortuous iliac artery in 10 of 11 patients in whom iliac dissections developed ipsilateral to primary component delivery. The results of our study suggest that a tortuosity index, defined as the sum of the curvature values measured every millimeter along the median luminal centerline of 0.3 cm^{-1} or greater, may be a reliable predictor of the risk of intimal injury along the access route following stent-graft delivery. While the risk of intimal injury is not the only factor in the determination of which side is most appropriate for the introduction of the primary limb of endovascular devices, quantification of iliac tortuosity prior to stent-graft deployment may aid in the selection of the appropriate access route, decreasing the rate of iliac dissections.

References

1. Joseph A, Ackerman D, Talley JD, Johnstone J, Kupersmith J. Manifestations of coronary atherosclerosis in young trauma victims: an autopsy study. J Am Coll Cardiol 1993; 22:459–467.
2. Ernst CB. Abdominal aortic aneurysm. N Engl J Med 1993; 328:1167–1172.
3. Zwiebel WJ. Aortic and iliac aneurysm. Semin Ultrasound CT MR 1992; 13:53–68.
4. Brown OW, Hollier LH, Pairolero PC, et al. Abdominal aortic aneurysm and coronary artery disease. Arch Surg 1981; 116: 1484–1488.
5. Zarins CK, Glagov S. Arterial wall pathology in atherosclerosis. In: Rutherford RB, ed. Vascular surgery. Philadelphia, Pa: Saunders, 1995; 204–221.
6. Bell DD, Gaspar MR. Routine aortography before abdominal aortic aneurysmectomy: a prospective study. Am J Surg 1982; 144:191–193.
7. Nuno IN, Collins GM, Bardin JA, et al. Should aortography be used routinely in the elective management of abdominal aortic aneurysm? Am J Surg 1982; 144: 53–57.
8. Johnston KW, Skobie TK. Multicenter prospective study of nonruptured abdominal aortic aneurysms. I. Population and operative management. J Vasc Surg 1988; 7:69–81.
9. Limpert JD, Vogelzang RL, Yao JST. Computed tomography of aortoiliac atherosclerosis. J Vasc Surg 1987; 5:814–819.
10. Beebe HG, Jackson T, Pigott JP. Aortic aneurysm morphology for planning en-

dovascular aortic grafts: limitations of conventional imaging methods. J Endovasc Surg 1995; 2:139–148.
11. Broeders IA, Blankensteijn JD, Olree M, Mali W, Eikelboom BC. Preoperative sizing of grafts for transfemoral endovascular aneurysm management: a prospective comparative study of spiral CT angiography, arteriography, and conventional CT imaging. J Endovasc Surg 1997; 4:252–261.
12. May J, White GH, Yu W, Waugh R, Stephen MS, Harris JP. Repair of abdominal aortic aneurysms by the endoluminal method: outcome in the first 100 patients. Med J Aust 1996; 165:549–551.
13. Chuter TA, Donayre C, Wendt G. Bifurcated stent-grafts for endovascular repair of abdominal aortic aneurysm: preliminary case reports. Surg Endosc 1994; 8: 800–802.
14. Parodi JC, Criado FJ, Barone HD, Schonholz C, Queral LA. Endoluminal aortic aneurysm repair using a balloon-expandable stent-graft device: a progress report. Ann Vasc Surg 1994; 8:523–529.
15. May J, White GH, Yu W, et al. Endoluminal grafting of abdominal aortic aneurysms: cause of failure and their prevention. J Endovasc Surg 1994; 1:44–52.
16. Dorffner R, Thurnher S, Polterauer P, Kretschmer G, Lammer J. Treatment of abdominal aortic aneurysms with transfemoral placement of stent-grafts: complications and secondary radiologic intervention. Radiology 1997; 204:79–86.
17. Blum U, Langer M, Spillner G, et al. Abdominal aortic aneurysms: preliminary technical and clinical results with transfemoral placement of endovascular self-expanding stent-grafts. Radiology 1996; 198:25–31.
18. Lorensen WE, Cline HE. Marching cubes: a high resolution 3D surface construction system. Comput Graph 1987; 21:163–169.
19. Paik DS, Beaulieu CF, Jeffrey RB, Rubin GD, Napel S. Automated flight path planning for virtual endoscopy. Med Phys 1998; 25:629–637.
20. Rubin GD, Paik DS, Johnston PC, Napel S. Measurement of the aorta and its branches with helical CT. Radiology 1998; 206:823–829.
21. Buckley JA, Shifrin RY, Paik DS, Rubin GD. Automated volumetric quantification of blood vessels using MR angiography (abstr). Radiology 1998; 209(P):475.
22. Becker GJ, Palmaz JC, Rees CR, et al. Angioplasty-induced dissections in human iliac arteries: management with Palmaz balloon-expandable intraluminal stents. Radiology 1990; 176:31–38.
23. Waller BF, Miller J, Morgan R, Tejada E. Atherosclerotic plaque calcific deposits: an important factor in success or failure of transluminal coronary angioplasty (TCA) (abstr). Circulation 1988; 78(suppl 2):376.
24. Gardiner GA, Meyerovitz MF, Harrington DP, et al. Dissection complicating angioplasty. AJR Am J Roentgenol 1985; 145: 627–631.
25. Chuter TA, Reilly LM. Surgical reconstruction of the iliac arteries prior to endovascular aortic aneurysm repair. J Endovasc Surg 1997; 4:307–311.
26. Parodi JC. Endovascular repair of abdominal aortic aneurysms and other arterial lesions. J Vasc Surg 1995; 21:549–557.